Journal of Materials and Environmental Science
ISSN : 2028-2508
e-ISSN : 2737-890X
CODEN : JMESCN

J. Mater. Environ. Sci., 2026, Volume 17, Issue 7, Page 1091-1108

http://www.jmaterenvironsci.com

Characterization of a clay soil from Côte d'Ivoire for use in green building

Garba Labo M. N. [1,2]*, Ibrahim Grema M. H. [1,2], Adamou Ibro A. [1], Kouassi E. K. A. [1], Amadou Kiari M. N.[1,2], Marou G. [3], Yao K. B.[1,2].

[1]Laboratoire des Procédés Industriels de Synthèse, de l'Environnement et des Energies Nouvelles (LAPISEN), Institut National Polytechnique Felix Houphouët Boigny (INP-HB), BP 1093, Yamoussoukro, Côte d'Ivoire
[2] Centre d'Excellence Africain pour la Valorisation des Déchets en Produits à Haute Valeur Ajoutée (CEA-VALOPRO), Institut National Polytechnique Félix Houphouët-Boigny (INP-HB), BP 1093, Yamoussoukro, Côte d'Ivoire
[3] Laboratoire Matériaux, Eaux et Environnement (LAMEE), Université Abdou Moumouni (UAM)- Faculté des Sciences et Techniques (FAST), BP 10896/237, Niamey, Niger

**Corresponding author, Email address: labo.garba21@inphb.ci, mahamannazirou92@gmail.com*

***Received** 18 May 2026,*
***Revised** 01 July 2026,*
***Accepted** 01 July 2026*

Keywords:
- ✓ *Côte d'Ivoire;*
- ✓ *Clay Soil;*
- ✓ *Characterization;*
- ✓ *Utilization;*
- ✓ *Green Building*

***Citation**: Garba Labo M. N., Ibrahim Grema M. H., Adamou Ibro A., Kouassi E. K. A., Amadou Kiari M. N., Marou G., Yao K. B. (2026) Characterization of a clay soil from Côte d'Ivoire for use in green building, J. Mater. Environ. Sci., 17(7), 1091-1108*

Abstract: This study focuses on the characterization of a clay soil (AGY) from the city of Yamoussoukro in central Côte d'Ivoire. The sample underwent physical, chemical, geotechnical, mineralogical, microstructural, and thermal characterization. The moisture content, loss on ignition, organic matter, and density were 0.92±0.02%, 9.65±0.03%, 0.86±0.15%, and 2.34±0.09%, respectively. The methylene blue value (VBS = 0.95 g/100g) falls within the range of sandy-loamy soils, which are moderately plastic and water-sensitive. The AGY sample consists mainly of silica (SiO_2: 63.76%) and alumina (Al_2O_3: 21.63%), to which is added a significant content of iron oxides (Fe_2O_3: 4.71%) and potassium (K_2O: 3.86%). Other oxides (CaO, TiO_2, MnO, P_2O_5 et SO_3) are present in smaller quantities. The mineralogical composition of the material is dominated by quartz (38.32%), followed by muscovite (32.69%) and kaolinite (22.92%), with a significant content of goethite (5.24%). The infrared spectrum revealed vibrational bands of the minerals identified by XRD (kaolinite, muscovite, goethite, and quartz). The morphology and microstructure (SEM/EDS) of the sample confirmed the presence of kaolinite and quartz in the sample, as well as its aluminosilicate nature. Given the results obtained and the absence of swelling clay minerals such as montmorillonites in the sample, AGY clay is suitable for the manufacture of earthen bricks.

1. Introduction

Urban growth in sub-Saharan Africa is increasing the demand for sustainable building materials, but the widespread use of concrete results in a high carbon footprint (Adadja *et al.*, 2020; Adu *et al.*, 2025). In this context, adobe bricks emerge as a more environmentally friendly local alternative. Beyond these socio-economic aspects, earthen materials offer advantageous hygrothermal properties that enhance indoor thermal comfort by regulating heat and moisture exchange (Fall *et al.*, 2021). However, despite the abundance of clay soils in Yamoussoukro, their use remains underutilized due to the variability of their properties. These variations directly influence their mechanical performance and durability (Bailly *et al.*, 2024). Recent studies show that stabilizing soils with alternative binders, such as agricultural waste ash or recycled materials, significantly improves their mechanical performance and durability while reducing their environmental impact (Kiebre *et al.,* 2025; Li *et al.,* 2024). These approaches align with the principles of the circular economy and the utilization of local resources. Despite these advantages, soil use in Côte d'Ivoire remains largely empirical, with a lack of scientific data specific to certain local contexts such as that of Yamoussoukro. Clay soils play a decisive role in the manufacture of compressed earth bricks by ensuring the material's cohesion. However, their high plasticity and sensitivity to water can impair performance, necessitating in-depth characterization (Akartasse *et al.,* 2022; Junaid Asghar *et al.,* 2024; Muñoz *et al.,* 2024; El Miz *et al.,* 2025; Dehmani *et al.,* 2026). This study examines clay soil from Yamoussoukro through a multiscale characterization (physical, chemical, mineralogical, morphological, geotechnical, thermal, and microstructural) to support the manufacture of earthen bricks for green building. The objective is to evaluate its intrinsic properties in order to identify its potential for use. The main hypothesis posits that physicochemical and mineralogical characteristics directly control the geotechnical and thermal behavior of soils. It is also assumed that the nature and proportion of clay minerals influence cohesion, plasticity, and durability. Finally, the microstructure and morphology of the particles are believed to be decisive in the mechanisms of heat transfer and mechanical strength.

2. Materials and Methodology

2.1. Sampling

The clay used in this study comes from the Yamoussoukro region, specifically from a site traditionally used by the local population for making adobe bricks. This choice is part of an effort to promote the use of local natural resources in sustainable building materials. The extraction site is located on the outskirts of Yamoussoukro/Assabou between latitude 6° 83'32.63'' North and longitude 5° 25'83.07'' West, at an elevation of 220.72 m. In the remainder of this study, this clay is designated by the acronym AGY. After extraction, AGY was crushed, air-dried, and then screened using a 3mm mesh to obtain a uniform particle size distribution. Geotechnical, physical, chemical, mineralogical, and thermal characterization was then performed to assess its quality and suitability for the manufacture of compressed earth bricks (CEB).

Figure 1. Sieve grid on the left and dried clay on the right

2.2. Physical Characterization

Moisture content

Moisture content (MC) refers to the amount of water contained in the material (Karunanithy *et al.,* 2013). In accordance with standard NF EN ISO 18134-1 (2016), it was determined as the weight loss of the sample in a drying oven at 105 °C. The moisture content was calculated using **Eqn. 1:**

$$MC\ (\%) = \frac{(m_1 - m_2)}{m_1} \times 100 \qquad \textbf{Eqn. 1}$$

With m_1 and m_2 be the respective masses of the sample before and after heating at 105 °C for 24 hours in the oven.

Loss on ignition

Loss on ignition (LOI) is the loss of mass resulting from the calcination of a material. In this study, the calcination temperature was 1000 °C for 2 hours. Loss on ignition is therefore the difference in mass of the sample before and after calcination, in accordance with the protocol of standard EN 196-2. It is calculated using the following **Eqn. 2:**

$$LOI = \frac{(m_2 - m_3)}{m_2} \times 100 \qquad \textbf{Eqn. 2}$$

With m_1 and m_2 be the respective masses of the sample before and after calcination.

Organic Matter Content

The organic matter (OM) content of AGY was determined using the method described by Staljanssens et al. (Staljanssens *et al.,* 1975). This method is based on the oxidation of organic matter using hydrogen peroxide. To do this, 100 g (m_0) of clay were suspended in a mixture consisting of 200 mL of distilled water and 20 mL of hydrogen peroxide, 10 volumes (3%). After 2 hours of reaction, the residue was dried at 105 °C to a constant mass (m_1) (Laibi *et al.,* 2017). The organic matter content was calculated using **Eqn. 3:**

$$OM\ (\%) = \frac{m_0 - m_1}{m_0} \times 100 \qquad \textbf{Eqn. 3}$$

m_0 (g): Initial mass of the clay sample before the reaction with hydrogen peroxide;
m_1 (g): mass of the sample after the reaction and dried at 105 °C for 24 hours.

Density

The density of the clay was determined using the water pycnometer method, following the protocol described by Gagea and Mirica (Gagea & Mirica, 1998). Five (5) g of powder with a particle size smaller than 63 µm were used for a four-step measurement. First, the water pycnometer was cleaned and dried, then weighed empty to obtain the empty mass m_1. Next, 5 g of the clay powder was placed in the pycnometer, and the mass of the assembly was measured and designated as m_2. Subsequently, the mass of the pycnometer containing the same amount of clay and filled with distilled water to the mark, while adjusting the mixture with a Pasteur pipette, was determined and recorded as m_3. Finally, the mass of the pycnometer alone, filled with distilled water, was determined and corresponds to m_4. The density of the sample is given by **Eqn. 4:**

$$\rho = \left[\frac{(m_2 - m_1) \times (\rho_L - \rho_a)}{m_4 + (m_2 - m_1) - m_3}\right] + \rho_a \qquad \textbf{Eqn. 4}$$

ρ ($g.cm^{-3}$): density of the clay; ρ_L ($g.cm^{-3}$): density of water (1 $g.cm^{-3}$); ρ_a ($g.cm^{-3}$): density of air (0,0012047 $g.cm^{-3}$); m_1 (g): mass of the empty pycnometer; m_2 (g): mass of the pycnometer with 5 g of clay; m_3 (g): mass of the pycnometer with the same amount of clay and filled with distilled water; m_4 (g): mass of the pycnometer filled with distilled water.

2.3. Geotechnical Characterization

Grain Size Analysis by Sieving and Sedimentation

The grain size analysis by sieving and sedimentation was performed in accordance with standards EN 933-1 and NF P94-057 at the Laboratory of Materials and Civil Engineering at the Technical University of Cluj-Napoca in Romania. Particle size analysis by sieving and sedimentation determines the size distribution of particles ranging from 8 mm to 0.125 mm, corresponding mainly to coarse sand, fine sand, and small gravel particles. First, the sample was dried at 105 °C for 24 hours. The 1000 g sample was placed in a column of standard sieves (8 mm, 4 mm, 2 mm, 1 mm, 0.5 mm, 0.25 mm, 0.125 mm). After mechanical sieving, the mass retained on each sieve was weighed and then expressed as a percentage of the total mass.

As for the sedimentation method, it was performed on particles smaller than 80 µm (silt and clay). After dispersion in a deflocculating solution, the particles settle according to their size in accordance with Stokes' law. Using a Robinson pipette, samples were taken at specific depths and time intervals, allowing the proportion of the various fine fractions to be calculated. The combination of these two methods provides a continuous particle size distribution curve covering all soil fractions, from gravel to clay, and forms the basis for the textural and mechanical classification of soils

Laser Particle Size Analysis

Laser particle size analysis was performed using the Fraunhofer model to determine the particle size distribution. The procedure involved immersing the sample for 15 seconds in distilled water used as a solvent. Aggregation in the resulting suspension was first reduced by ultrasonic treatment in the apparatus prior to particle size analysis. The instrument used to study the particle size distribution of the clay is a Shimadzu Sald-7101 laser particle size analyzer. The analyses were performed at the Research Center for Computer-Aided Process Engineering at Babes Bolyai University in Cluj-Napoca, Romania.

Atterberg Limits

The Atterberg limits (liquid limit, plastic limit, plasticity index) are used to characterize the consistency of fine-grained soils by distinguishing between three physical states: liquid, plastic, and solid. These limits were determined using the Casagrande method in accordance with French standard NF P 94-051 (AFNOR, 1993) at the Laboratory of Chemistry and Renewable Energies (LaCER) at Nazi BONI University in Bobo Dioulasso (Burkina Faso). The liquid limit (W_L) and plasticity limit (W_P) were measured using the Casagrande box method, while the plasticity index (IP) was calculated by taking the difference between W_L and W_P (**Eqn. 5**):

$$I_P = W_L - W_P \qquad \textbf{Eqn. 5}$$

Methylene Blue Value (MBV)

The methylene blue test measures the adsorption capacity of soils based on the quantity and nature of their clay fraction. It involves suspending 30 to 60 g of soil in 500 mL of demineralized water, then gradually adding a methylene blue solution (10 g/L) while stirring. After each addition, a drop of the suspension is placed on filter paper: clay saturation is reached when the central blue spot is surrounded by a pale halo, indicating an excess of dye. This marks the end of the test. The test was conducted in accordance with standard NF P 94-068 (Khlif, 2024) at the Laboratory of Chemistry and Renewable Energies (LaCER) at Nazi BONI University in Bobo Dioulasso (Burkina Faso). The methylene blue value is determined by **Eqn. 6:**

$$MBV = 100 \times \frac{\frac{B}{M}}{1+W} \qquad \textbf{Eqn. 6}$$

MBV (g/100): methylene blue value; M: mass of the material used for the test; W: initial moisture content; and B: mass of methylene blue used.

2.4. Chemical Characterization (XRF)

The chemical composition of the clay sample in terms of oxides was determined by X-ray fluorescence spectrometry using a Panalytical Epsilon 4 EDXRF spectrometer. The analysis was performed at the Central Laboratory of Umaru Musa Yar'Adua University in Katsina State, Nigeria.

2.5. Mineralogical Characterization

X-ray Diffraction

The mineralogical composition was determined by X-ray diffraction (XRD). This technique is used to identify the nature of crystalline and amorphous species present on the surface of materials. The analysis was performed at the X-Techlab Laboratory in Sèmè City (Benin) using a diffractometer powder X-ray (Panalyan) operating at 45 kV and 40 mA. These PXRD analyses were performed using the monochromatic radiation of CuKα radiation (λ = 1.54056). These phases were identified using HighScore software and a PDF database (powder diffraction files) from the ICDD (International Center for Diffraction Data).

Fourier Transform Infrared

Fourier transform infrared (FTIR) spectroscopy is used to identify functional groups present on the surface of materials. The analyses were performed using an Agilent Cary 630 FTIR spectrophotometer, in a wavenumber range from 4000 to 650 cm^{-1}.

Semi-quantitative analysis

Combining chemical analysis with X-ray diffraction makes it possible to quantify the percentage of mineral phases present in the sample using the calculation method proposed by Yvon et al. (Yvon *et al.,* 1982):

$$\mathbf{T(a) = \sum M_i P_i(a)} \qquad \textbf{Eqn. 7}$$

T(a): percentage (%) content of oxide “a” in the sample; Mi: percentage (%) content of mineral “i” in the sample; Pi(a): proportion of oxide “a” in mineral ‘i’ (this proportion is derived from the ideal formula assigned to mineral “i”).

2.6. Thermogravimetric Analysis Coupled with Differential Thermal Analysis

Thermogravimetric analysis (TGA) and differential thermal analysis (DTA), performed simultaneously using a PerkinElmer instrument, allow, respectively, for monitoring changes in sample mass and detecting associated endothermic or exothermic phenomena. Approximately 13.294 mg were heated from 30 °C to 950 °C in a nitrogen atmosphere at a heating rate of 10 °C/min. DTA is generated in parallel as the reciprocal calorimetric response of TGA. The analysis was performed at the University of Kaduna Laboratory in the Federal Republic of Nigeria.

2.7. Morphological and Microstructural Characteristics

Scanning electron microscopy coupled with energy-dispersive X-ray spectroscopy (SEM/EDS) was performed using a Phenom ProX scanning electron microscope (Phenom World, Eindhoven, Netherlands). The analysis was conducted at the University of Kaduna in the Federal Republic of Nigeria.

3. Results and Discussion

3.1. Physical Properties

The results of the physical properties of AGY are presented in **Table 1**. The table shows a moisture content of 0.92±0.02% for the clay. This value indicates that the clay sample is only minimally hydrated by atmospheric water (Bodian *et al.*, 2018; Taïpabé *et al.*, 2025). The value recorded in the present study is much lower than that reported by Bodian et al. for a clay from Senegal, which is 4.78% (Bodian *et al.*, 2021). According to these authors, variations in natural moisture content may be related to the amount of fine or clayey particles contained in the analyzed samples (Bodian *et al.*, 2021).

The loss on ignition of the clay is 9.65±0.03%. This value is lower than that expected for pure kaolinite, which is around 14% (Kouamé *et al.,* 2021). This loss on ignition is likely due to the dehydroxylation of clay minerals, the oxidation of organic matter, and the decomposition of carbonates and hydroxides present in the sample studied (Kagonbé *et al.*, 2021).

The organic matter content in the clay is 0.86±0.15% and is less than 2%. The low organic matter content indicates that the clay is inorganic from a geotechnical perspective (Taïpabé *et al.,* 2025). This is favorable for the stabilization and durability of the formulated bricks, as low organic matter values have a negligible effect on the production processes of earthen bricks (Taïpabé *et al.*, 2025).

The density of the clay studied is 2.34±0.09 $g.cm^{-3}$. This value is close to those generally reported in the literature for clays (Aboudi Mana *et al.*, 2017; Méité *et al.*, 2021). Similar density values have been reported in the literature: 2.65 (Amon *et al.,* 2017), 2.6 (Méité *et al.,* 2021), 2.50-2.55 (Nwosu *et al.,* 2018), 2.06-2.73 (Damian *et al.,* 2021).

Table 1. Physical parameters of clay

MC (%)	LOI (%)	OM (%)	Density (g/cm^3)
0.92±0.02	9.65±0.03	0.86±0.15	2.34±0.09

3.2. Geotechnical Characterization

Grain Size Analysis by Sieving and Sedimentation

Knowledge of a soil's particle size distribution is essential for evaluating its suitability as a construction material (Darman *et al.,* 2022), such as in the manufacture of rammed earth blocks (REB). **Figure 2** shows the mechanical particle size distribution curve for AGY. The analysis was performed on particles passing through a 3mm sieve. Analysis of **Figure 2** reveals a distribution that is highly concentrated in the intermediate fractions, characterized by a significant retention peak between 600 and 700 µm, indicating a polymodal particle size distribution dominated by medium-sized particles. The rapid decrease in retention percentages toward the higher particle size classes indicates a near absence of coarse particles, while the cumulative percentage passing curve reaches nearly 100% before 2-3 mm. This confirms that the material is composed primarily of fine to medium-sized particles. This particle size distribution suggests a predominantly sandy material, with slight dispersion toward the extremes, a relatively narrow distribution, and a homogeneous texture centered on intermediate sizes.

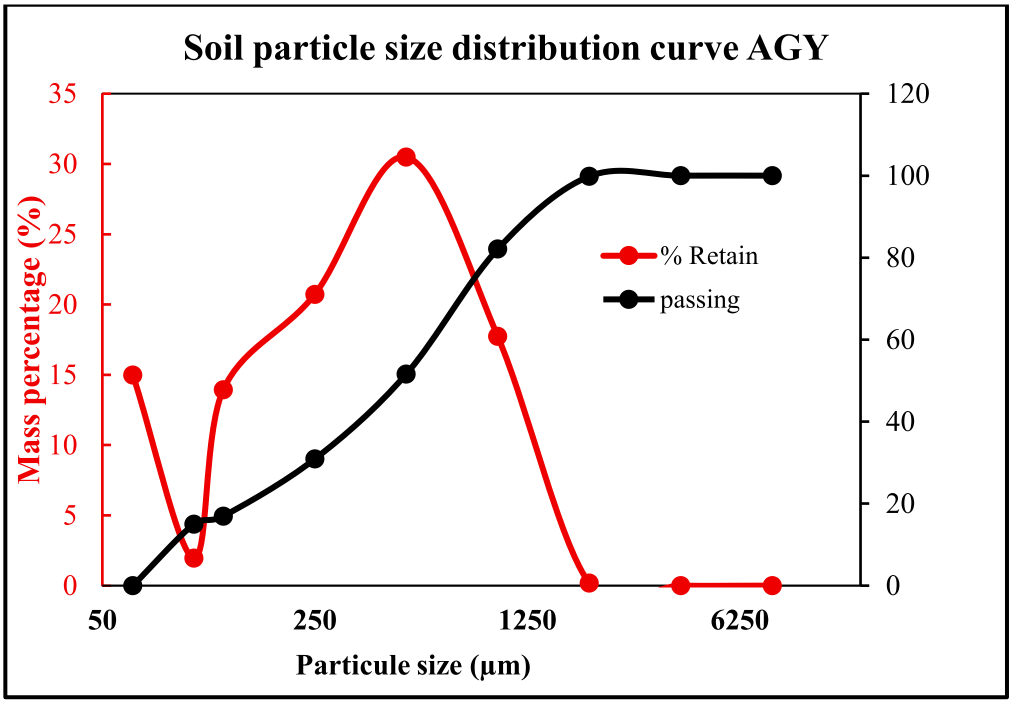

Figure 1. Mechanical particle size distribution curve

The sedimentation method complements the mechanical particle size analysis. It allows for the determination of the proportion of particles of different sizes (clay, silt, sand) suspended in a hexametaphosphate-based deflocculation solution. The results are presented in **Table 2**.

Table 2. Particle size distribution of AGY

Clay	Fine silt	Coarse silt	Fine sand	Coarse sand
8.05	19.5	17	16.01	39.4

An analysis of **Table 2** reveals that AGY consists of 8.05% clay, 19.5% fine silt, 17% coarse silt, 16.01% fine sand, and 39.4% coarse sand. These results are consistent with the requirements of the ARS-680 standard for the manufacture of BTC, which specifies sand, silt, and clay contents ranging from 25% to 80%, 10% to 25%, and 8% to 30%, respectively (Nshimiyimana *et al.*, 2020).

Laser Particle Size Analysis

Laser particle size analysis has already been used by several authors to estimate the particle size of powdered materials (Méité *et al.*, 2024). **Figure 3** shows the volume (red curve) and cumulative (black curve) particle size distributions of AGY clay. The volumetric curve of AGY indicates several grain populations, which is characteristic of a non-uniform soil. A first peak between 0.3 and 5 µm corresponds to the fine clay and silt fraction. The other peaks are located around 10 µm (silty fraction), 40 µm, and 114 µm (sandy fraction). As for the cumulative curve, it rises gradually with a transition around 10 µm indicating a high contribution of silt and an inflection around 60 to 100 µm corresponding to the increase in the sandy fraction. This shows that this soil consists of a mixture of fine (clay/silt), medium, and sandy particles, typical of a sandy-silt soil with a dominant proportion of fine to medium sand, containing enough silt to influence its behavior (low plasticity, low cohesion, and intermediate compactness) (Tan *et al.*, 2017). The cumulative volume curves of the sample allowed us to determine the maximum diameters corresponding to given cumulative volumes. The values corresponding to 10% (d_{10}); 50% (d_{50}); and 90% (d_{90}) of the AGY grains are shown in **Table 3**. These different values indicate a broad grain size distribution in the sample. The d_{10} value of AGY, which is less than 2 µm (1.53 µm), confirms the actual presence of clay phases in the sample. The relatively low d_{50} value (10.02 µm) indicates the fineness of the grains constituting the samples. Finally, the relatively high d_{90} value is likely due to the significant amount of sand contained in the AGY clay.

Table 2. Main particle size parameters of AGY

Clay	d_{10} (µm)	d_{50} (µm)	d_{90} (µm)
AGY	1.53	10.02	75.72

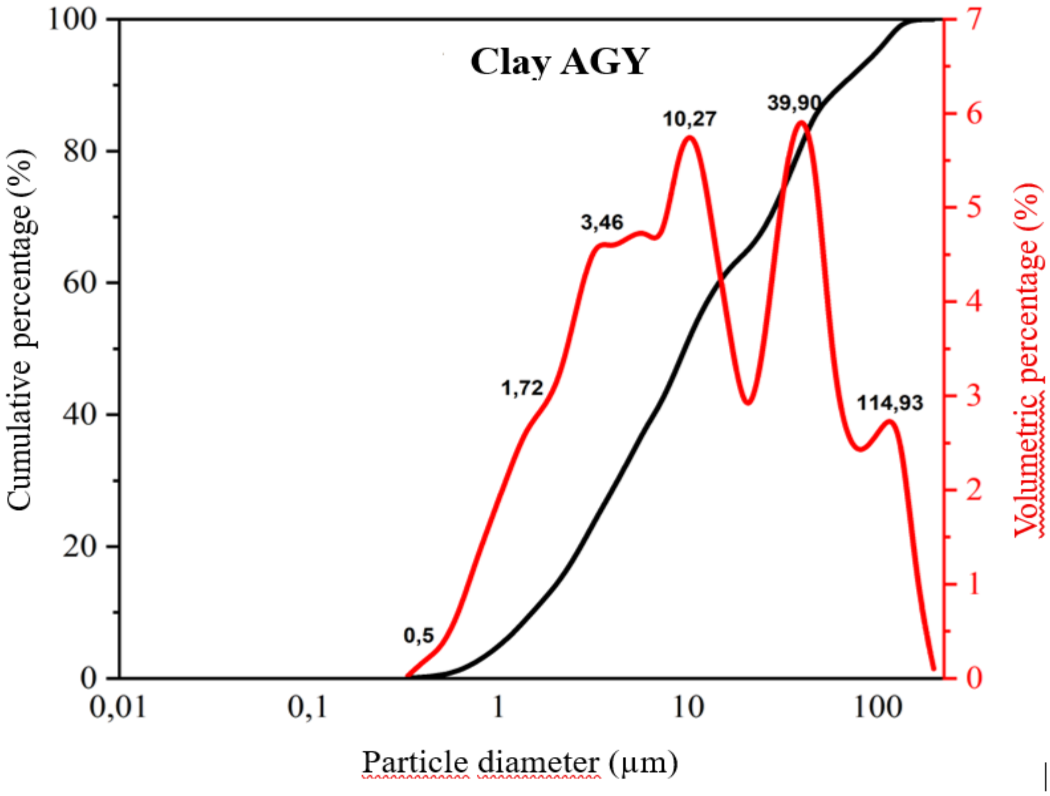

Figure 2. Laser particle size distribution of AGY

Atterberg Limits

The results of the Atterberg limits for AGY are presented in **Table 4**. The clay's liquid limit is 39.5%. This value is less than 40% ($W_L < 40\%$), which is the recommended value for the stabilization of earth blocks (Burroughs, 2008) The liquid limit of AGY therefore suggests that it can be used for the production of earthen bricks. The plasticity limit (29.5%) of the sample is higher than the maximum value of the plasticity limit range (16 - 19%) favorable for the stabilization of earth blocks (Burroughs, 2008). This high plasticity limit could result in high shrinkage limit values (Rimbarngaye *et al.,* 2022). The plasticity index (I_P) of the clay is 10%, a value outside the plastic range, which is $15 \leq I_P \leq 45$ (Boussen *et al.,* 2016).

The W_L and I_P values plotted on the Casagrande plasticity diagram (**Figure 4**) place the sample below line A, with a W_L of less than 50%, classifying it as inorganic silt or slightly plastic organic soil. This interpretation is consistent with the sedimentation-based particle size analysis results, which indicate a low clay content of 8.05%, insufficient to confer significant plasticity. Similarly, the laser diffraction particle size analysis results confirm this classification (d_{10} = 1.5 µm), showing a highly present fine fraction that is predominantly silty. Taken together, these results indicate a material with low plasticity, moderate cohesion, and limited reactivity to water characteristics typical of low-plasticity silts (Chrétien et al., 2007; Yoshimitsu et al., 2019).

Table 3. Limits of Atterberg

Echantillon	AGY
Liquidity limit W_L	39.5%
Plasticity limit W_P	29.5%
Plasticity index $I_P = W_L - W_P$	10%

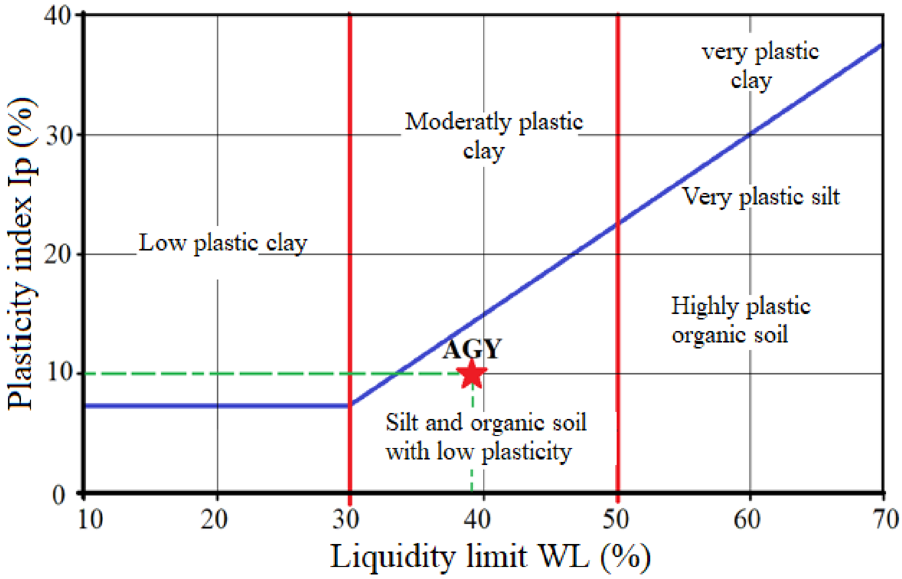

Figure 3. Position of the clay studied in the Casagrande plasticity abacus

Methylene Blue Value

The methylene blue value (MBV) of the sample under study is 0.95 g/100 g. This value indicates that the material under study is a sandy-loam soil that is water-sensitive, as it falls within the range $0.2 \leq MBV \leq 1.5$ (I. Sanou, 2017). Furthermore, the MBV value is relatively low. This could indicate low activity of the clay fraction and suggest an absence of swelling clay minerals in the sample (Kouamé *et al.*, 2021; Latifi *et al.,* 2025; Taïpabé *et al.,* 2025). This result is consistent with the results of the granulometric analysis and the Atterberg limits regarding the nature of the soil.

3.3. Chemical Composition

The chemical composition of the AGY sample in terms of oxides, as determined by XRF, is presented in **Table 5**. Analysis of this table reveals that the AGY sample is composed primarily of silica (SiO_2) and alumina (Al_2O_3), confirming its classification within the aluminosilicate family (Rehman *et al.,* 2021). The SiO_2/Al_2O_3 mass ratio, estimated at 2.95, is higher than that of pure kaolins (≈1.18), indicating the presence of a substantial amount of free silica as well as other clay minerals (Sorgho *et al.,* 2016). The high iron oxide (Fe_2O_3) content suggests the presence of iron oxides or hydroxides, such as goethite (Nshimiyimana *et al.*, 2020). Furthermore, the potassium oxide (K_2O) content may be linked to the presence of mica phases, notably illite or muscovite, while the absence of sodium oxide (Na_2O) may indicate the absence of feldspar phases. The significant amount of calcium oxide (CaO) may be due to the presence of carbonate phases or traces of calcium minerals. These results are consistent with the conclusions of (Brahima, 2013; Dao *et al.,* 2018; I. Sanou *et al.,* 2024).

Table 4. Chemical composition of AGY

SiO_2	Al_2O_3	Fe_2O_3	TiO_2	MgO	CaO	K_2O	Na_2O	P_2O_5	MnO	SO_3	SiO_2/Al_2O_3
63.76	21.63	4.71	1.56	0	2.36	3.86	-	0.22	0.08	0.25	2.95

3.4. Mineralogical Characteristics of the Clay

X-ray Diffraction

The results of the X-ray diffraction mineralogical analysis of AGY are presented in **Figure 5**. Analysis of the diffractogram shows that the sample consists mainly of kaolinite ($Al_22Si_2O_5(OH)_4$), muscovite $KAl_3Si_3O_{10}(OH)_2$), quartz (SiO_2), and goethite ($FeO(OH)$. The presence of kaolinite could give the soil significant plasticity, thereby facilitating the molding and compaction of the bricks (Sawadogo *et al.*, 2026). Muscovite, for its part, can improve the mechanical strength of the bricks thanks to its crystalline layers. Quartz, a hard and abrasive mineral, can influence the bricks' resistance to wear and abrasion. As for goethite, it can affect the color and durability of the bricks (Sawadogo *et al.*, 2026). The absence of swelling clay minerals such as smectites in the diffractogram confirms the results of the physical and geotechnical characterization. Furthermore, this absence of smectite-type minerals is an advantage for using the sample as a construction material, as the presence of these clay minerals in materials used for geotechnical purposes influences their properties, particularly their water absorption and swelling (Taïpabé *et al.,* 2025).

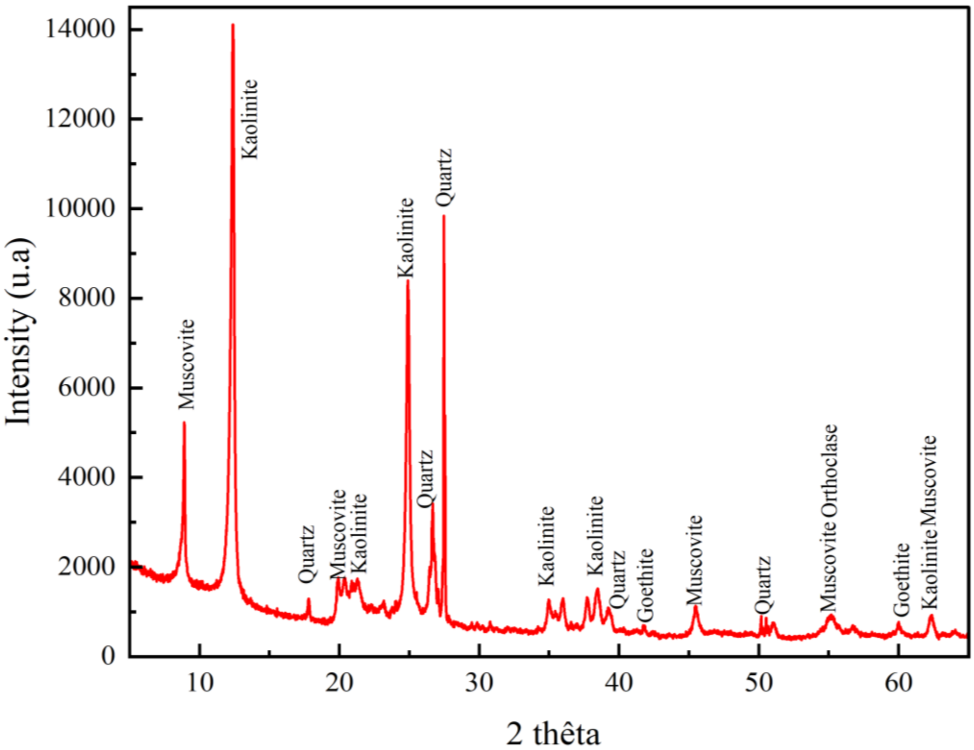

Figure 5. X-ray diffraction pattern of AGY

Fourier-transform infrared spectroscopy

Figure 6 shows the infrared spectrum of AGY clay, recorded in the 4000–400 cm^{-1} frequency range. The infrared bands in the AGY spectrum were identified based on data from the literature (Brahima, 2013; Kouka Amed, 2019; Mohamed, 2009; Ntimugura *et al.,* 2017; Rouxhet *et al.,* 1977; I. Sanou *et al.,* 2024a; I. Sanou *et al.,* 2024b ; Younoussa, 2008). In the high-frequency region (3000-4000 cm^{-1}), the bands observed at 3686, 3649, and 3613 cm^{-1} are characteristic of the valence vibrations of the hydroxyl groups in kaolinite. The first two correspond to the external hydroxyl groups, while the last is associated with the internal hydroxyl groups, located between the tetrahedral and octahedral layers. This last band can also be attributed to muscovite. In the (700-1200 cm^{-1}) region, the Si-O and Al-O vibrations appear. The following bands are also identified on the AGY diffractogram:

The bands around 1111, 1021, and 992 cm^{-1} are attributed to $Si-O$ valence vibrations, notably the asymmetric Si-O-Si mode, characteristic of kaolinite and quartz.

The band at 788 cm^{-1} is characteristics of the in-plane Al-O-Si deformation vibration, typical of muscovite and potentially of quartz.

The band at 905 cm^{-1} is associated with the deformation vibration of the Al-OH bonds in kaolinite.

The bands at 697.11 and 668 cm^{-1} are attributed, respectively, to the OH valence vibrations of kaolinite and the Si-O valence vibrations of quartz, as well as to the $Si-O-Si$ bending vibration.

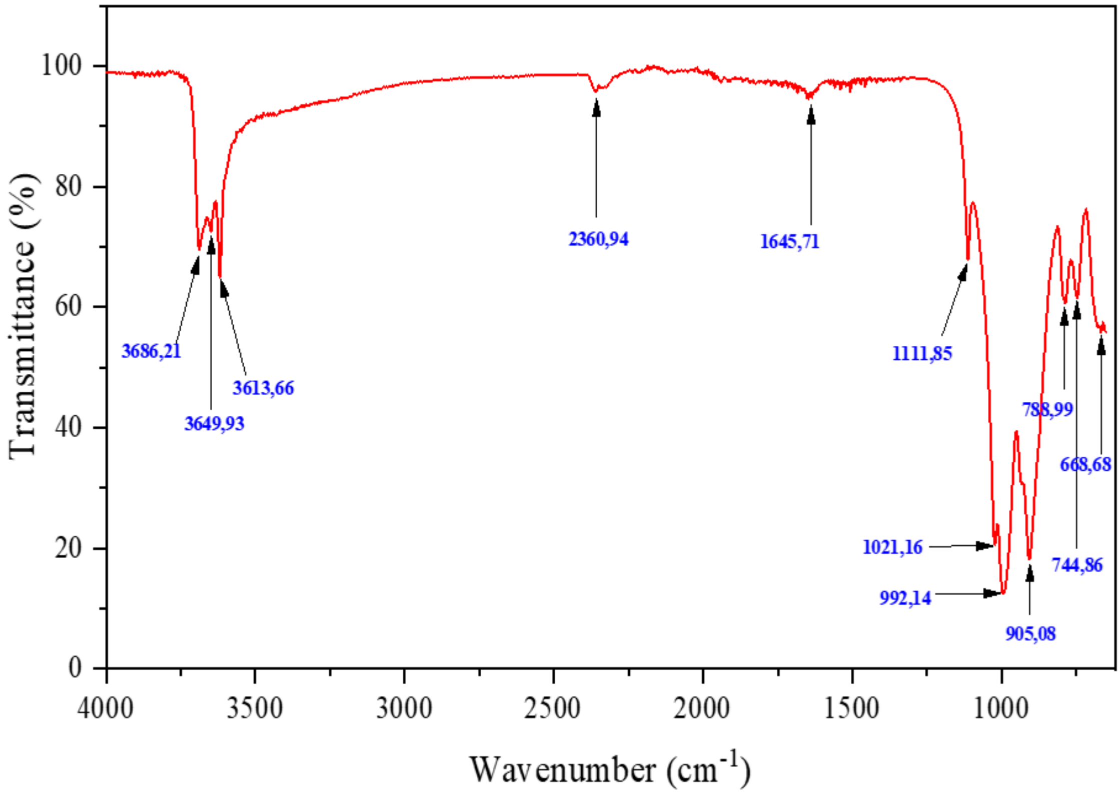

Figure 6. AGY Infrared Spectrum

3.5. Thermal Properties

Figure 7 shows the results of the ATG/DTG thermal analysis of AGY. Examination of this figure reveals several mass losses. The first mass loss (0.14%), observed between 30 and 150 °C, is attributed to the release of hygroscopic water initially present in the sample. The second loss, occurring between 150 and 360 °C (0.93%), could be due to the dehydration of iron oxyhydroxides, leading to the transformation of goethite into hematite (Bodian *et al.*, 2018; Brahima, 2013; Dao *et al.*, 2018; I. Sanou *et al.*, 2024a). The mass loss observed between 360 and 550 °C (1.05%) corresponds to the dehydroxylation of clay minerals, particularly kaolinite, whose structural hydroxyl groups are removed, leading to the destruction of the crystal lattice and the formation of metakaolinite (Méité *et al.*, 2022; I. Sanou *et al.*, 2024a). The dehydroxylation of ordered kaolinite occurs around 600 °C; the lower temperature observed in the sample indicates the presence of disordered kaolinite (Dao *et al.*, 2018). The final mass loss, between 550 and 900 °C (0.12%), can be attributed to the decomposition of organic matter and small carbonate phases ($MgCO_3$), as well as to the decarbonation of residual carbonates (Millogo *et al.,* 2008).

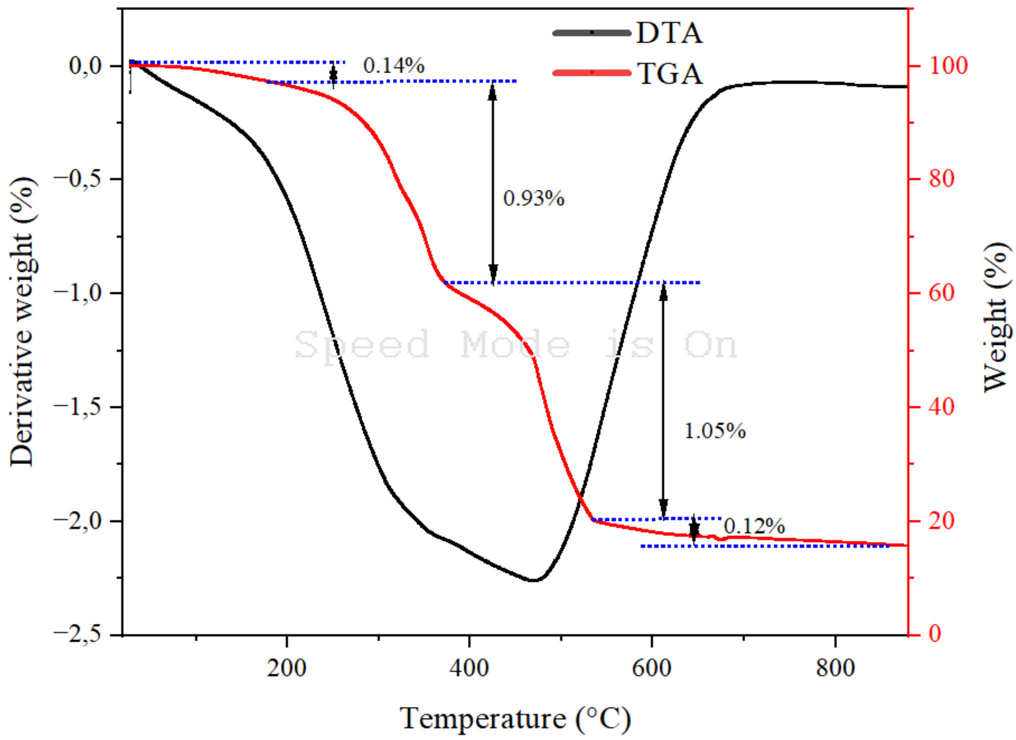

Figure 7. AGY's ATG/DTG curves

3.6. Mineralogical Semi-Quantification

By combining chemical analysis with mineralogy using the relationship established by Yvon et al. (Yvon *et al.,* 1982), we were able to determine the percentage of each mineral present in the sample. The semi-quantitative approach was based on the following approximations:

- Alumina (Al_2O_3) is contained in kaolinite and muscovite;
- Silica (SiO_2) is distributed among kaolinite, muscovite, and quartz;
- Iron oxide (Fe_2O_3) is entirely attributed to goethite;
- Potassium oxide (K_2O) is entirely attributed to muscovite.

Based on the above approximations, the mass percentages of the minerals were estimated using the following equations (**Eqn. 8, Eqn. 9, Eqn. 10, Eqn. 11**):

- $\%\mathrm{Goethite} = \frac{\%\mathrm{Fe_2O_3}\ \mathrm{x}\ 2\mathrm{M_{Goethite}}}{\mathrm{M_{Fe_2O_3}}}$ **Eqn. 8**
- $\%\mathrm{Muscovite} = \frac{\%\mathrm{K_2O}\ \mathrm{x}\ 2\mathrm{M_{Muscovite}}}{\mathrm{M_{K_2O}}}$ **Eqn. 9**
- $\%\mathrm{Kaolinite} = \left(\frac{\%\mathrm{Al_2O_3}}{\mathrm{M_{Al_2O_3}}} - \frac{3}{2}\mathrm{x}\frac{\%\mathrm{Muscovite}}{\mathrm{M_{Muscovite}}}\right)\ \mathrm{x}\ \mathrm{M_{Kaolinite}}$ **Eqn. 10**
- $\%\mathrm{Quartz} = \%\mathrm{SiO_2} - \left(\frac{2\ \mathrm{x}\ \%\mathrm{Kaolinite}}{\mathrm{M_{Kaolinite}}} + \frac{6}{2}\mathrm{x}\frac{\%\mathrm{Muscovite}}{\mathrm{M_{Muscovite}}} + \frac{6}{2}\mathrm{x}\frac{\%\mathrm{Albite}}{\mathrm{M_{Albite}}}\right)\ \mathrm{x}\ \mathrm{M_{SiO_2}}$ **Eqn. 11**

Table 6 presents the results of the semi-quantification. These results show that the sample is rich in clay minerals (kaolinite and muscovite) and quartz, with a significant content of goethite. Indeed, AGY consists of 22.92% kaolinite, 32.69% muscovite, 5.24% goethite, and 38.32% quartz. Kaolinite is known for its low water absorption capacity, and its prevalence in materials used for making clay bricks enhances their molding properties (Kamga Djoumen *et al.,* 2023). The significant amount of quartz (38.32%) in the sample is the source of free silica, as indicated by the chemical analysis through the high SiO_2/Al_2O_3 ratio. This high quartz content acts to de-grease the kaolinite (Kouamé *et al.,* 2021). The balance, which is 0.83%, consists mainly of amorphous minerals and/or, above all, organic matter (I. Sanou *et al.,* 2024). The mineralogical composition is consistent with the results of the physical and geotechnical properties.

Table 6. Mineralogical composition of clay

Minerals	Kaolinite	Muscovite	Goethite	Quartz	Total	Balance
% mass	22.92	32.69	5.24	38.32	99.17	0.83

3.7. Morphological and Microstructural Characteristics

SEM micrographs of AGY obtained at different magnifications (100, 80, and 40 µm) are shown in Figure 8. SEM observations reveal particles in the form of aggregates of irregular platelets, typical of kaolinites (Issaka, 2022; Qlihaa *et al.,* 2016). These platelets, often stacked, can exhibit hexagonal shapes on the order of micrometers. Similar observations have been made by several authors on clay materials containing kaolinite (Fort et al., 2024; Gauly *et al.,* 2025; A. Sanou *et al.,* 2024; Soro *et al.,* 2023). The presence of platelets of varying sizes and morphologies suggests the coexistence of muscovite (Delavernhe, 2011). The inclusions present in AGY could be attributed to goethite (Mohamed, 2009). At the same time, the characteristic polyhedra of quartz are clearly identifiable in the SEM images, confirming the XRD results (Brahima, 2013; Qlihaa *et al.,* 2016). The results of the energy-dispersive X-ray analysis are shown in **Figure 9**. Analysis of the AGY EDS diagram reveals high silicon (48.01%) and aluminum (36.9%) contents, as well as significant amounts of iron (3.24%), potassium (3.73%), sodium (2.58%), and potassium (2.32%). These results are consistent with the presence of quartz, kaolinite, muscovite, and goethite identified by X-ray diffraction. This method made it possible to detect sodium and magnesium, which had not been detected previously.

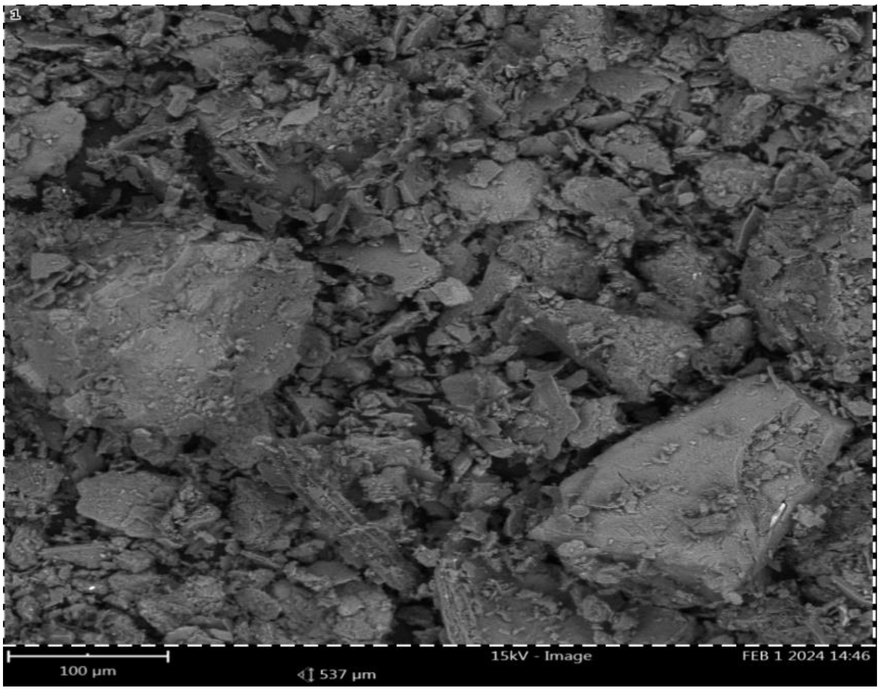

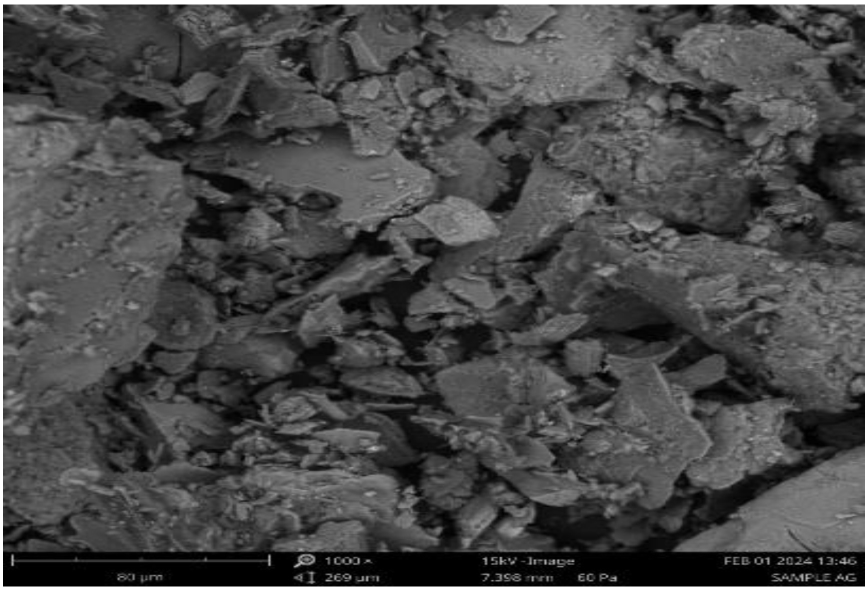

Figure 8. Micrograph of AGY

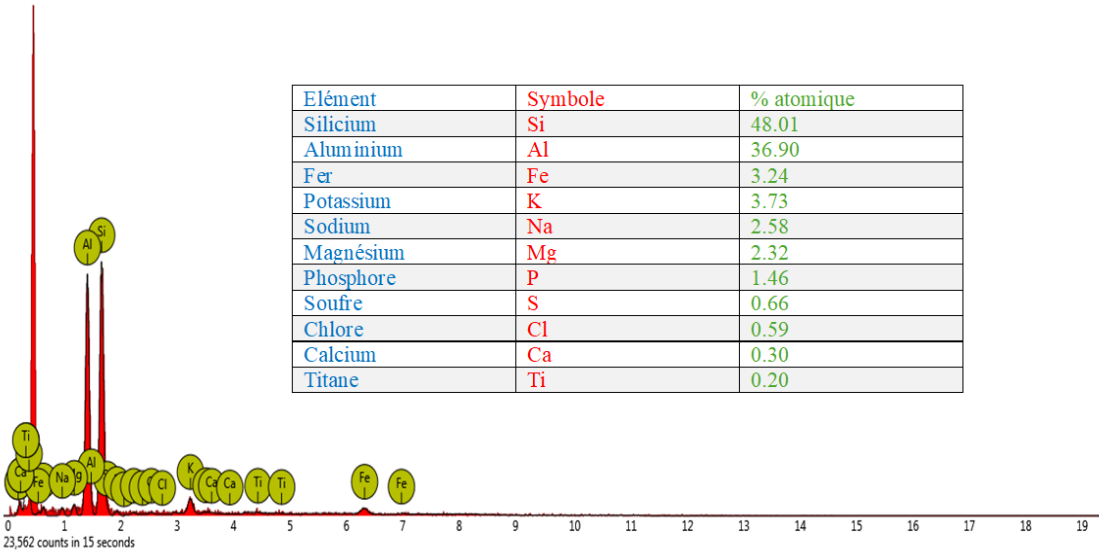

Elément	Symbole	% atomique
Silicium	Si	48.01
Aluminium	Al	36.90
Fer	Fe	3.24
Potassium	K	3.73
Sodium	Na	2.58
Magnésium	Mg	2.32
Phosphore	P	1.46
Soufre	S	0.66
Chlore	Cl	0.59
Calcium	Ca	0.30
Titane	Ti	0.20

Figure 9. EDS spectrum of AGY

Conclusion

The objective of this study was to characterize a clay from Côte d'Ivoire with a view to its use in green building. The combined results of the physical, geotechnical, chemical, mineralogical, microstructural, and thermal analyses, supplemented by mineralogical semi-quantification, provided a comprehensive understanding of the soil under study. These analyses showed that it is a sandy-silt soil containing 55% sand, 36% silt, and 8% clay, moderately plastic (Ip = 10%), water-sensitive (MBV = 0.95 g/100g), and inorganic. It is an aluminosilicate, dominated by quartz (38.32%), muscovite (32.69%), and kaolinite (22.92%) with a significant content of goethite (5.24%). This soil could therefore offer an interesting structure but requires stabilization to achieve sufficient strength. The low clay content limits natural cohesion and makes the material vulnerable to moisture, hence the need to add cement to improve compactness and durability. However, the exclusive use of cement increases the carbon footprint. Partially substituting cement with a suitable ash allows for a reduction in CO_2 emissions while maintaining, or even improving, mechanical performance, making this soil more sustainable and effective for construction.

Acknowledgements: Garba Labo M. N. would like to thank the African Centre of Excellence for the Valorization of Waste into High Value-Added Products (CEA-VALOPRO) for its financial support. He also acknowledges the financial support by Eugen Ionescu fellowship 2024-2025 offered by Agence Universitaire de la Francophonie (AUF) and The Romanian Government. The authors thank the XTechLab laboratory in Sémé City (Cotonou) in Benin.

Disclosure statement: *Conflict of Interest:* The authors declare that there are no conflicts of interest.

Compliance with Ethical Standards: This article does not contain any studies involving human or animal subjects.

References

Aboudi Mana S. C., Hanafiah M. M., & Chowdhury A. J. K. (2017) Environmental characteristics of clay and clay-based minerals, *Geology, Ecology, and Landscapes*, 1(3), 155-161. https://doi.org/10.1080/24749508.2017.1361128

Adadja C. E., Houngan C. A., Koutsawa Y., Khelil A., Vianou A., Gbaguidi V., Zahrouni H., Gibigaye M., & Hattab M. (2020) Modélisation multi-échelles des propriétés élastiques du composite argile-pailles de riz [PhD Thesis, EPAC/UAC]. https://theses.fr/api/v1/document/2020LORR0067

Adu T. F., Zebilila M. D. H., Adzakey P., Ofori Sarkodie W., & Mustapha Z. (2025) Life cycle embodied carbon evaluation of a two-bedroom house construction in Ghana : A comparison between stabilized laterite and sancrete building, *Heliyon,* 11(3), e42212. https://doi.org/10.1016/j.heliyon.2025.e42212

AFNOR (1993) NF P 94-051, Sols : Reconnaissance et Essais-Détermination des Limites d'Atterberg. Limite de Liquidité à la Coupelle-Limite de Plasticité au Rouleau (Norme française NF P 94-051; p. 16). Association Française de Normalisation.

Akartasse N., Azzaoui K., Mejdoubi E., Hammouti B., Elansari L.L., Abou-salama M., Aaddouz M., Sabbahi R., Rhazi L., Siaj M. (2022), Environmental-friendly adsorbent composite based on hydroxyapatite/hydroxypropyl methyl-cellulose for removal of cationic dyes from an aqueous solution, *Polymers,* 14(11), 2147, https://doi.org/10.3390/polym14112147

Amon L. N., Konan L. K., Goure-Doubi H., Andji J. Y. Y., Coulibaly J. K., & Oyetola S. (2017) Physico-chemical and structural properties of clay-based ceramic filters from Côte d'Ivoire, *Journal de La Société Ouest-Africaine de Chimie*, 44(1), 70-77.

Bailly G. C., El Mendili Y., Konin A., & Khoury E. (2024) Advancing Earth-Based Construction : A Comprehensive Review of Stabilization and Reinforcement Techniques for Adobe and Compressed Earth Blocks, *Eng*, 5(2), Article 2. https://doi.org/10.3390/eng5020041

Bodian S., Faye, M., Sambou V., Séne N. A., Diaw I., & Faye K. (2021) Caractérisation physico-chimique des matières premières argileuses de la carrière de Thicky (Sénégal) pour la fabrication de briques en terre, *Journal de Physique de la SOAPHYS*, 3(1), 1-7. https://doi.org/10.46411/jpsoaphys.2021.01.01

Bodian S., Faye M., Sene N. A., Sambou V., Limam O., & Thiam A. (2018) Thermo-mechanical behavior of unfired bricks and fired bricks made from a mixture of clay soil and laterite, *Journal of Building Engineering*, 18, 172-179. https://doi.org/10.1016/j.jobe.2018.03.014

Boussen S., Sghaier D., Chaabani F., Jamoussi B., & Bennour A. (2016) Characteristics and industrial application of the Lower Cretaceous clay deposits (Bouhedma Formation), Southeast Tunisia : Potential use for the manufacturing of ceramic tiles and bricks, *Applied Clay Science*, 123, 210-221. https://doi.org/10.1016/j.clay.2016.01.027

Brahima S. (2013) Caractérisation et valorisation de quelques argiles du Burkina Faso : Application au traitement des eaux et aux géomatériaux de construction [These de doctorat]. Université de Ouagadougou

Burroughs S. (2008) Soil Property Criteria for Rammed Earth Stabilization, *Journal of Materials in Civil Engineering*, 20(3), 264-273. https://doi.org/10.1061/(ASCE)0899-1561(2008)20:3(264)

Chrétien M., Fabre R., Denis A., & Marache A. (2007) Recherche des paramètres d'identification géotechnique optimaux pour une classification des sols sensibles au retrait-gonflement, *Revue Française de Géotechnique*, (120-121), Article 120-121. https://doi.org/10.1051/geotech/2007120091

Damian G., Damian F., Szakács Z., Iepure G., & Aştefanei D. (2021) Mineralogical and Physico-Chemical Characterization of the Oraşu-Nou (Romania) Bentonite Resources, *Minerals*, 11(9), 938. https://doi.org/10.3390/min11090938

Dao K., Ouedraogo M., Millogo Y., Aubert J.-E., & Gomina M. (2018) Thermal, hydric and mechanical behaviours of adobes stabilized with cement, *Construction and Building Materials*, 158, 84-96. https://doi.org/10.1016/j.conbuildmat.2017.10.001

Dehmani Y., Bentahar I., Lgaz H., El-Kordy A., Aldalbahi A., Alrashdi A.A., Dehbi A., Lamhasni T., Hammouti B., Sadik A. (2026) A critical review of natural clay minerals: Structural characterization, textural properties, and adsorption mechanisms for sustainable wastewater treatment, *Materials Today Advances,* 29, 2026, 100682, ISSN 2590-0498, https://doi.org/10.1016/j.mtadv.2025.100682

Delavernhe L. (2011) Étude multi-échelle de la réactivité des altérites lors du traitement à la chaux [Phdthesis, Université de Nantes]. https://theses.hal.science/tel-00671340

El Miz M., Loutou M., Aaddouz M., Tahani A., Mejdoubi E., Jodeh S., Azzaoui K., Hammouti B. (2024) Thermal release of Thymol encapsulated into sodium, organic and pillared modified clay matrixes, *Chemical Papers,* 78, 1585–1599, https://doi.org/10.1007/s11696-023-03186-4

Fall M., Sarr D., Cissé E. M., & Konaté D. (2021) Physico-mechanical characterization of clay and laterite bricks stabilized or not with cement, *Open Journal of Civil Engineering*, 11(01), 60-69. https://www.academia.edu/download/121646101/PaperDownload.pdf

Fort C. I., Sanou A., Coulibaly M., Yao K. B., & Turdean G. L. (2024) Green modified electrode for sensitive simultaneous heavy metal ions electrodetection, *Sensors and Actuators B: Chemical*, 418, 136326. https://doi.org/10.1016/j.snb.2024.136326

Gagea L., & Mirica E. (1998), *Chimia fizica si ingineria sistemelor oxidice*. QUO VADIS.

Gauly L. P., Coulibaly M., Soro S. B., Kouadio K. S., N'Dri S. R., Sanou A., & Trokourey A. (2025) Characterization and enhanced performance of Ivorian clays as potential modifiers in carbon paste electrodes, *Discover Applied Sciences*, 7(2), 128. https://doi.org/10.1007/s42452-024-06457-1

Issaka G. (2022) Contribution à l'étude des organo-argiles : Synthèse, caractérisations physicochimiques et application à l'adsorption du bisphénol A. Université Joseph KI-ZERBO.

Junaid A., Muhammad Y. S., Riaz U. R., & Muhammad Umair. (2024) Investigation on the use of natural soil stabilizers for compressed earth bricks, *World Journal of Advanced Engineering Technology and Sciences*, 13(2), 435-439. https://doi.org/10.30574/wjaets.2024.13.2.0586

Kagonbé B. P., Tsozué D., Nzeukou A. N., & Ngos S. (2021) Mineralogical, physico-chemical and ceramic properties of clay materials from Sekandé and Gashiga (North, Cameroon) and their suitability in earthenware production, *Heliyon*, 7(7). https://doi.org/10.1016/j.heliyon.2021.e07608

Kamga Djoumen T., Tiomo I. F., Vouffo M., Ngapgue F., Sali M., Keubou V.W.T. (2023) Characterization of basaltic rock laterites in Dschang, West-Cameroon: Compressed Earth Bricks (CEB) for low-cost buildings, *Case Studies in Construction Materials*, 19, e02335. https://doi.org/10.1016/j.cscm.2023.e02335

Karunanithy C., Muthukumarappan K., & Donepudi A. (2013) Moisture Sorption Characteristics of Corn Stover and Big Bluestem, *Journal of Renewable Energy*, 2013, e939504. https://doi.org/10.1155/2013/939504

Khlif N. (2024, décembre 25) Détermination de La Valeur de Bleu de Méthylène-Learning Geotechnique. https://learninggeotechnique.com/%20determination-la-valeur-de-bleu-de-methylene

Kiebre R., Ouedraogo E., Sawadogo N. J., Sayouba K., Kiebre R., Ouedraogo E., Sawadogo N. J., Sayouba K. (2025) Impact of rice biomass and cement stabilization on the mechanical and thermal properties of compressed soil bricks, In *2025 IEEE Multi-Conference on Natural and Engineering Sciences for Sahel's Sustainable Development, MNE3SD* 2025. https://doi.org/10.1109/mne3sd67637.2025.11323246

Kouamé A. N., Konan L. K., & Doubi B. I. H. G. (2021) Microstructure and Mineralogy of Compressed Earth Bricks Incorporating Shea Butter Wastes Stabilized with Cement, *Advances in Materials*, 10(4), 67-74. https://doi.org/10.11648/j.am.20211004.13

Kouka Amed J. O. (2019) Stabilisation de matériaux de construction durables et écologiques à base de terre crue par des liants organiques et/ou minéraux à faibles impacts environnementaux [Université Paul Sabatier - Toulouse III, ffNNT : 2019TOU30199ff. fftel- 02628530]. https://tel.archives-ouvertes.

Laibi A. B., Gomina M., Sorgho B., Sagbo E., Blanchart P., Boutouil M., & Sohounhloule D. K. C. (2017) Caractérisation physico-chimique et géotechnique de deux sites argileux du Bénin en vue de leur valorisation dans l'éco-construction, *International Journal of Biological and Chemical Sciences*, 11(1), 499-514. https://doi.org/10.4314/ijbcs.v11i1.40

Latifi S., Saoiabi S., Alanazi M. M., Boukra O., Krime A., El Hammari L., Azzaoui K., Hammouti B., Hanbali G., Jodeh S., Saoiabi A., Sabbahi R., Algarra M., Abidi N. (2025) Low-Cost Titania-Hydroxyapatite (TiHAp) nanocomposites were synthesized for removal of Methylene blue under Solar and UV irradiation, *Next Materials*, 8, 100859, ISSN 2949-8228, https://doi.org/10.1016/j.nxmate.2025.100859

Li B., Luo F., Li, X., & Liu J. (2024) Mechanical properties evolution of clays treated with rice husk ash subjected to freezing-thawing cycles. *Case Studies in Construction Materials*, *20*, e02712. https://doi.org/10.1016/j.cscm.2023.e02712

Méité N., Konan L. K., Tognonvi M. T., Doubi B. I. H. G., Gomina M., & Oyetola S. (2021) Properties of hydric and biodegradability of cassava starch-based bioplastics reinforced with thermally modified kaolin, *Carbohydrate Polymers*, 254, 117322. https://doi.org/10.1016/j.carbpol.2020.117322

Méité N., Konan L. K., Tognonvi M. T., & Oyetola S. (2022) Effect of metakaolin content on mechanical and water barrier properties of cassava starch films, *South African Journal of Chemical Engineering*, 40, 186-194. https://doi.org/10.1016/j.sajce.2022.03.005

Méité N., Zoro E. G., Doubi B. I. H. G., Sanou A., Kouakou L. P. M.-S., Fenzl N., do Canto Lopes L. O., & Konan L. K. (2024) Ageing, optical and life-cycle analysis of clay-reinforced cassava starch biocomposites. *Results in Chemistry*, 11, 101853. https://doi.org/10.1016/j.rechem.2024.101853

Millogo Y., Hajjaji M., & Ouedraogo R. (2008) Microstructure and physical properties of lime-clayey adobe bricks, *Construction and Building Materials*, 22(12), 2386-2392. https://doi.org/10.1016/j.conbuildmat.2007.09.002

Mohamed S. (2009). Caracterisation de matieres premieres argileuses des sites de Loulouka et de Korona (Burkina Faso) : Valorisation dans la céramique du carreau. Universite de Ouagadougou.

Muñoz S., Rojas M., Villena L., Tepe V., Garcia J., & Alvarez J. (2024) Physical and mechanical characterization of cement-stabilized compressed earth bricks, *Revista ingeniería de construcción*, 39(1), 85-95. https://doi.org/10.7764/ric.00101.21

Nshimiyimana P., Fagel, N., Messan A., Wetshondo D. O., & Courard L. (2020) Physico-chemical and mineralogical characterization of clay materials suitable for production of stabilized compressed earth blocks, *Construction and Building Materials*, 241, 118097. https://doi.org/10.1016/j.conbuildmat.2020.118097

Nshimiyimana P., Messan A., & Courard L. (2020) Physico-Mechanical and Hygro-Thermal Properties of Compressed Earth Blocks Stabilized with Industrial and Agro By-Product Binders. *Materials*, 13(17), 3769. https://doi.org/10.3390/ma13173769

Ntimugura F., Sore S. O., Bello L., & Messan A. (2017) The Influence of Metakaolin from Saaba (Burkina Faso) over Physico-Mechanical and Durability Properties of Mortars, *Open Journal of Civil Engineering*, 7(3), Article 3. https://doi.org/10.4236/ojce.2017.73027

Nwosu F. O., Ajala O. J., Owoyemi R. M., & Raheem B. G. (2018) Preparation and characterization of adsorbents derived from bentonite and kaolin clays, *Applied Water Science*, 8(7), 195. https://doi.org/10.1007/s13201-018-0827-2

Qlihaa A., Dhimni S., Melrhaka F., Hajjaji N., & Srhiri A. (2016) Caractérisation physico-chimique d'une argile Marocaine [Physico-chemical characterization of a morrocan clay].

Rehman M. U., Manan A., Uzair M., Khan A. S., Ullah A., Ahmad A. S., Wazir A. H., Qazi I., & Khan M. A. (2021) Physicochemical characterization of Pakistani clay for adsorption of methylene blue : Kinetic, isotherm and thermodynamic study, *Materials Chemistry and Physics*, 269, 124722.

Rimbarngaye A., Mwero J.N., Ronoh E.K. (2022) Effect of gum Arabic content on maximum dry density and optimum moisture content of laterite soil, *Heliyon*, 8(11). https://doi.org/10.1016/j.heliyon.2022.e11553

Rouxhet P. G., Samudacheata N., Jacobs H., & Anton O. (1977) Attribution of the OH stretching bands of kaolinite, *Clay Minerals*, 12(2), 171-179. https://doi.org/10.1180/claymin.1977.012.02.07

Sanou A., Coulibaly M., N'dri S. R., Tămaș T. L., Bizo L., Frentiu T., Covaci E., Abro K. D. M., Dablé P. J.-M. R., Yao K. B., Fort C. I., & Turdean G. L. (2024) Raw clay material-based modified carbon paste electrodes for sensitive heavy metal detection in drinking water, *Journal of Materials Science*, 59(30), 13961-13977. https://doi.org/10.1007/s10853-024-09945-2

Sanou I. (2017) Influence du mélange ciment-pouzzolane sur quelques propriétés physiques et mécaniques des adobes [Thèse de Doctorat]. Université Ouaga I Pr Joseph KI-ZERBO.

Sanou I., Ouedraogo M., Bamogo H., Meité N., Seynou M., Aubert J.-E., & Millogo Y. (2024a) Microstructural, physical, and mechanical characteristics of adobes amended with cement-metakaolin mixtures, *Emergent Materials*, 7(3), 1203-1217. https://doi.org/10.1007/s42247-024-00638-9

Sanou I., Zoungrana S., Ouedraogo M., Sanou A., & Millogo Y. (2024b) Evaluation of the Pozzolanic Activity of Metakaolin, Glass Powder and Silica Powder for Use in Cementitious Mortars, *Studia UBB Chemia* LXIX(4), 49–66. DOI:10.24193/subbchem.2024.4.04

Sawadogo Y., Ouattara S., Barry K., Sory N., Sawadogo M., Seynou M., Blanchart P., & Zerbo L. (2026) Physicochemical and Mineralogical Characteristics of Geopolymer Formulated from Kaolinitic Clay, *Journal of Materials Science Research*, 15(1), p9. https://doi.org/10.5539/jmsr.v15n1p9

Sorgho B., Bressollier P., Guel B., Zerbo L., Ouedraogo R., Gomina M., & Blanchart P. (2016) Étude des propriétés mécaniques des géomateriaux argileux associant la décoction de *Parkia Biglobosa* (néré), *Comptes Rendus. Chimie*, 19(7), 895-901. https://doi.org/10.1016/j.crci.2016.01.016

Soro S. B., Coulibaly M., Paul Gauly L., N'Dri S. R., Sanou A., & Trokourey A. (2023) Characterization of Clay Materials from Côte d'Ivoire : Possible Application for the Electrochemical Analysis, *Journal of Materials Science Research*, 12(1), 51-64. https://doi.org/10.5539/jmsr.v12n1p51

Staljanssens M., Marcoen J.-M., Fabry J., & Rassel A. (1975) Destruction de la matière organique par calcination à basse température en vue de l'analyse minéralogique des sols, *Annales de la Société Géologique de Belgique*, 98, 393-403.

Taïpabé D., Doko K. V., Datchossa T. A., Abdourahamane A. I., Mandela T., Sanou A., & Gibigaye M. (2025) Characterization of a lateritic soil in Chad with a view to its use in eco-construction, *J. Mater. Environ. Sci.,* 16 (7), 1189, 1209.

Tan X., Liu F., Hu L., Reed A. H., Furukawa Y., & Zhang G. (2017) Evaluation of the particle sizes of four clay minerals, *Applied Clay Science*, 135, 313-324. https://doi.org/10.1016/j.clay.2016.10.012

Yoshimitsu Y., Takashi T., Nyan M. K., Tatsuru A., Moe M. S. H., & Ryota H. (2019) A study on physical and mechanical properties for soft to firm clays in Yangon area – Properties of clays deposit at the sedimentary basins in Myanmar, *ResearchGate*. https://doi.org/10.1016/j.sandf.2019.05.008

Younoussa M. (2008) Etude géotechnique, chimique et minéralogique de matières premières argileuse et latéritique du Burkina Faso améliorées aux liants hydrauliques : Application au génie civil (bâtiment et route). Thèse de doctorat de l'Université de Ouagadougou.

Yvon J., Liétard O., Cases J.-M., & Delon J.-F. (1982) Minéralogie des argiles kaoliniques des Charentes, *Bulletin de Minéralogie*, 105(5), 431-437. https://doi.org/10.3406/bulmi.1982.7565

(2026) ; http://www.jmaterenvironsci.com